

## **SOME DEVELOPMENTS IN DYNAMIC FRACTURE MECHANICS**

S. de Luna, L. Rubio, J.L. Pérez-Castellanos, J. Fernández-Sáez and C. Navarro

Department of Mechanical Engineering, Carlos III University of Madrid,  
Avda. de la Universidad, 30. 28911. Leganés. Madrid. Spain.

### **ABSTRACT**

Recent developments in dynamic fracture mechanics at the Carlos III University of Madrid are summarised in this paper. They are grouped into two categories: (1) dynamic fracture of ductile materials at intermediate strain rates and (2) experimental techniques (dynamic bending test) to measure fracture parameters at high strain rates. In the first field of research, the influence of the strain rate on the dynamic fracture toughness and blunting process are investigated experimentally and numerically. The experimental analyses consisted in low-blow impact tests using a Charpy instrumented pendulum. Full numerical analyses of the tests were made using a simple micromechanical ductile damage model to explain the influence of the strain rate. For the second part of the study, a special experimental device for bending test at high strain rates, based on the Split Hopkinson Pressure Bar technique, was designed and constructed. A system of high speed photography technique was used to measure CMOD during the test directly from the images. Assuming an elastic behaviour for the material, the dynamic fracture initiation toughness could be obtained from the CMOD measurements just at the beginning of the crack propagation.

### **INTRODUCTION**

Mechanical integrity studies based on Fracture Mechanics of structural components require the knowledge of fracture properties of the materials involved. These properties are commonly obtained from laboratory tests in which the real operating conditions (loading rate, temperature, environment, etc) are reproduced. The knowledge of the dynamic fracture behaviour of the materials and the corresponding material properties, are of particular interest to engineers because many components are subjected to dynamic loads during normal operation of the component or through accidental causes. Therefore, tests are required to determine the dynamic fracture properties of the materials, but no test standards are available at present although different European Organisms (ESIS, DYMAT) are making important progress in this field.

This work outlines recent developments at Carlos III University of Madrid in Dynamic Fracture Mechanics. The paper is divided into two parts. First, experimental and numerical studies of the fracture process for a ductile material to explain the influence of strain rate on fracture initiation toughness of the material and to analyse the blunting process in dynamic conditions. Second, some recent achievements in the field of the dynamic bending test at high strain rates are presented. The experimental setup developed was based on a modified Split Hopkinson Pressure Bar and a system of high speed photography technique to measure the displacements at different points of the specimen directly from the images. From these displacements, and assuming that the material presented elastic behaviour, the dynamic fracture initiation toughness could be obtained.

### **DUCTILE FRACTURE OF STEELS AT INTERMEDIATE STRAIN RATES.**

The fracture initiation toughness for ductile materials is usually defined as the value of the J-integral at the onset of crack propagation. In these materials the crack tip, which presents an initial sharp shape, becomes blunted as a consequence of the strong strain field that appears in that zone. During this process (called blunting

process), the crack seems to grow although there is no new fracture surfaces. The curve relating the J-integral to the apparent crack growth is conventionally known as the blunting line.

As a result of any fracture test of the material, a curve relating  $J$ -integral with crack growth,  $\Delta a$ , can be drawn, usually referred to as the  $J$ - $\Delta a$  curve, The value of the  $J$ -integral fracture parameter at crack growth initiation can be determined from the intersection of this curve with the blunting line. In static fracture tests, a straight blunting line is normally assumed, its slope calculated from the material properties measured in static tensile tests [1, 2]. However, in dynamic loading conditions, no definite conclusions about the shape of the blunting line have yet been reached. MacGillivray and Lenkey [3] proposed using the same expression as that of the static case, with the material properties obtained from dynamic tensile tests. With this assumption, the blunting line in dynamic conditions is again a straight line, like in the static case, but with different slope. A more physical-based method to obtain the crack initiation fracture toughness, called in this paper  $J_{SZW}$ , could be by intersecting the experimental  $J$ - $\Delta a$  curve with a vertical line for a value of  $\Delta a$  equal to the stretch zone width (SZW). However this method does not give information as to the shape of the blunting line. An apparent blunting line slope from experiments would be deduced as the ratio between  $J_{SZW}$  and the SZW value. On the other hand, the fracture toughness of the material is affected by the loading rate [4, 5]. In ductile materials, with a fracture mechanism primarily controlled by the strain field, this property increases with the loading rate [4]. To explain these phenomena, micromechanical damage models are usually required to understand the fracture process.

### Material and experimental work

In this work the effect of the loading rate on the fracture toughness in Mode I of the commercial steel API-X70 [6], widely used in pipelines, is studied. This steel is a low carbon steel microalloyed with Al and Nb with the chemical composition given in Table 1.

TABLE 1  
CHEMICAL COMPOSITION OF THE STEEL API X70

C	Mn	Si	Ni	Cr	Cu	S	P	Mo	Nb	Va	Ti
0.1	1.75	0.39	<0.05	<0.05	0.1	<0.02	0.029	0.13	0.025	0.03	0.025

Its mechanical properties in static conditions, obtained from conventional tensile tests at strain rate,  $\dot{\epsilon}_0$ , about  $0.02 \text{ s}^{-1}$ , were: yield stress,  $\sigma_y = 520 \text{ MPa}$  and Ultimate Tensile Stress,  $\sigma_u = 600 \text{ MPa}$ . Additional dynamic tests were performed using the Split Hopkinson Pressure Bar at a strain rate of about  $700 \text{ s}^{-1}$ . In these conditions the properties were  $\sigma_y = 715 \text{ MPa}$ , and  $\sigma_u = 820 \text{ MPa}$ . From all these parameters, a constitutive equation valid at room temperature conditions could be established:

$$\sigma_e = E \epsilon_e \quad (\text{for } \sigma_e < \sigma_0) \quad (1)$$

$$\sigma_e = \left( \frac{\dot{\epsilon}_e}{\dot{\epsilon}_0} \right)^m \cdot \sigma_0 \cdot \epsilon_e^n \quad (\text{for } \sigma_e > \sigma_0) \quad (2)$$

where  $\sigma_e$  is the Von Mises equivalent stress,  $\epsilon_e$  the total equivalent strain,  $E$  the Young's modulus,  $\sigma_0$  a reference stress,  $\dot{\epsilon}_e$  the equivalent strain rate,  $\dot{\epsilon}_0$  the equivalent strain rate in static conditions, and  $m$  and  $n$  are two material constants,  $n$  being the strain hardening exponent. The values of these material parameters are given in Table 2.

TABLE 2  
PARAMETERS OF THE CONSTITUTIVE EQUATION

E (GPa)	$\sigma_0$ (MPa)	$\dot{\epsilon}_0$ (s <sup>-1</sup> )	m	n
210	500	0.02	0.03	0.08

Two types of Mode I fracture tests were performed with this material to study its behaviour at different loading rates: dynamic three-point bending tests at low impact velocity (low-blow tests) and quasi-static three-point bending tests. In all the tests, standard V-notch Charpy-size specimens, with an initial crack generated by fatigue in an Instron device Mod. 8516, were used. Pre-cracking of the specimen was carried out according to the EGF P1-90 standard [2]. After fatigue pre-cracking, the specimens were sidegrooved to promote straight-fronted ductile crack growth during the test. The depth of the sidegrooving was 1 mm, so the net section thickness,  $B_n$ , became 8 mm. In the case of dynamic loading, the specimens were tested in an instrumented Charpy pendulum (Ceast Mod. CH-E/30A) at hammer impact velocities ranging from 0.5 to 0.9 m s<sup>-1</sup>. From the measured time history of the load exerted by the hammer on the specimen,  $F(t)$ , the velocity,  $v(t)$ , and displacement,  $s(t)$ , time histories for the hammer, and taking into account the system compliance, the displacement of the load application point of the specimen,  $s_c(t)$  and the energy absorbed by it,  $E_a$ , during the test can be calculated [7]. The  $J$ -integral is evaluated by the expression [2]:

$$J = \frac{2E_a}{B_n(W - a_0)} \quad (3)$$

where  $B_n$  y  $W$  are, respectively, the net thickness and the width of the specimen, and  $a_0$  the initial crack length. For the quasi-static three-point bending tests the load was applied at constant velocity to reach pre-determined displacements of the load application point, which ensured stable crack growth in each test. The  $J$ -integral was also calculated from Eq. (3), computing the absorbed energy,  $E_a$ , from the curve  $F-s_c$  but now for the static test. The load application point displacement,  $s_c$ , was measured with an LVDT extensometer. After the static and dynamic tests, the specimens were placed in an electric furnace to oxidize the surface of the crack generated by fatigue, as well as that appearing from the ductile crack growth. Then they were immersed in liquid nitrogen and broken in a brittle manner. The initial crack length, the crack growth, and the stretch zone width were measured according to the EGF P1-90 standard [2]. From the points  $(J, \Delta a)$  experimentally found in each test (static or dynamic), the best power fit curve was calculated, according to standard EGF P1-90 [2], as:

$$J = A(\Delta a + C)^D \quad (4)$$

Several fracture parameters, using different criteria, were obtained from the fitted curve as, for instance,  $J_{0.2}$  (the  $J$ -value corresponding to 0.2 mm crack growth) and  $J_{SZW}$  ( $J$ -value for  $\Delta a = SZW$ ).

### Numerical simulation

The numerical analyses of the specimens, in both static and dynamic conditions, were carried out using the FEM multipurpose commercial computer code ABAQUS [8]. An updated Lagrangian formulation was adopted to take into account the finite deformations and rotations that appear in the problem. In the dynamic test simulations, finite element meshes for the specimen and for the hammer were used. For the dynamic loading case, four initial impact velocities 0.50, 0.56, 0.66 and 0.70 m/s were imposed on all the nodes of the hammer. The crack lengths considered were respectively: 5.54, 6.10, 5.80 and 5.86 mm. For the static case, a displacement at the force application point and in the load direction was imposed. One simulation was carried out in this case and only the specimen was modelled. The final displacement of the load application point and the crack length were, respectively: 1.20 mm and 5.60 mm. The material presented ductile fracture behaviour, the fracture process being a consequence of the growth and the coalescence of microvoids. Rice and Tracey [9] proposed a simple model for the growth of a spherical microvoid of initial radius  $R_0$ , in three-dimensional stress fields, in which the radius at any time of the microvoid,  $R$ , may be obtained [9]:

$$\ln \frac{R}{R_0} = \int_0^{\epsilon_p} 0.283 \exp\left(\frac{3}{2} \cdot \frac{\sigma_H}{\sigma_e}\right) d\epsilon_p \quad (5)$$

A damage variable,  $D$ , can be defined using this micromechanical model as:

$$D = \ln\left(\frac{R}{R_0}\right) \quad (6)$$

In the numerical simulations and once the load is applied, it is assumed that crack growth takes place when the variable  $D$ , at the proximity of the crack tip, reaches a critical value,  $D_{crit}$ , which is assumed to be a strain rate independent material property. Once this condition is satisfied, and the crack is going to grow, the value of the  $J$ -integral can be computed, which gives a measure of the fracture initiation toughness of the material. The damage variable value was computed far enough from the crack tip to avoid a possible unreal numerical distortion as a consequence of the large plastic deformation at this zone. Since the numerical model does not consider the crack growth, the  $J$ -integral versus the damage variable curves obtained with this model has only physical meaning until the onset of crack propagation. From numerical simulation of any test, the  $J$ -integral and the crack mouth opening displacement, CMOD, parameters during the crack tip blunting process may be obtained and thus the relationship between them. The crack tip opening displacement, CTOD, can be computed, in turn, from the CMOD as [2]:

$$CTOD = \frac{K^2(1-\nu^2)}{2E\sigma_y} + \frac{0.4(W-a_0)}{(0.4W+0.6a_0)} V_p \quad (7)$$

where  $K$  is the stress intensity factor of a three-point bending specimen loaded at its middle section,  $\nu$  the material Poisson ratio,  $\sigma_y$  the yield stress, and  $V_p$  is the plastic component of the CMOD at a specific time. CTOD may also be expressed as a function of the apparent crack growth,  $\Delta a$ , assuming that the same relationship as that of the static case ( $CTOD = 2.5 \Delta a$ ) applies in dynamic conditions. So a blunting line,  $J$ - $\Delta a$ , could be constructed from the numerical results.

### Results and discussion

Figure 1 shows the relationship between the  $J$ -integral and the damage variable in the dynamic tests at different impact velocities, and also for the static test. Very small differences are observed between the curves corresponding to dynamic conditions, although they differ from those of the quasi-static test. This shows that low blow tests are appropriate to obtain the dynamic fracture toughness at intermediate strain rates. From the simulations, the slope of the blunting line (named “numerical blunting line” in this paper) may be obtained as previously explained. Figure 2 shows the numerical blunting lines for dynamic (impact velocity of 0.56 m/s) and static simulated tests. The slope of the line in dynamic conditions is higher than that of the static test. From the  $J$ - $\Delta a$  fitted curve, different fracture toughness parameters were obtained for both static and dynamic conditions:  $J_{0.2}$  and  $J_{SZW}$ , as defined before, and  $J^*_{SZW}$ , which is the  $J$ -value on the numerical blunting line for  $\Delta a = SZW$ . For dynamic conditions, the results were:  $SZW = 45 \mu m$ ,  $J_{0.2} = 151 \text{ kJ/m}^2$ ,  $J_{SZW} = 80 \text{ kJ/m}^2$  and  $J^*_{SZW} = 90 \text{ kJ/m}^2$ . For the static case, these parameters were:  $SZW = 45 \mu m$ ,  $J_{0.2} = 123 \text{ kJ/m}^2$ ,  $J_{SZW} = 76 \text{ kJ/m}^2$  and  $J^*_{SZW} = 70 \text{ kJ/m}^2$ .

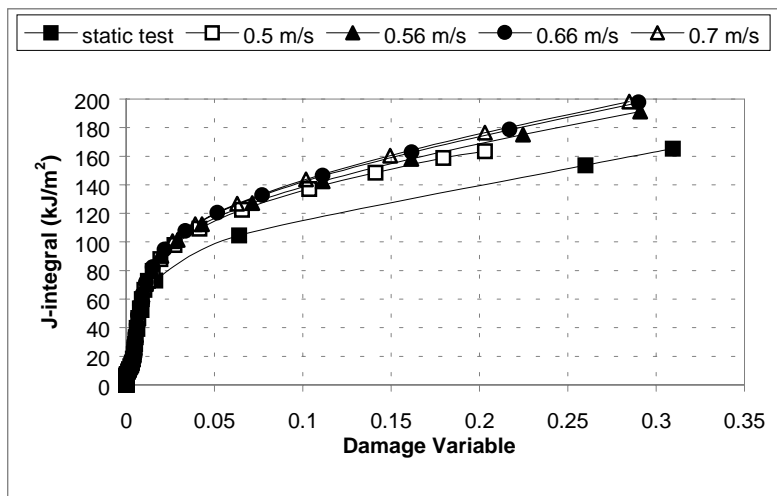
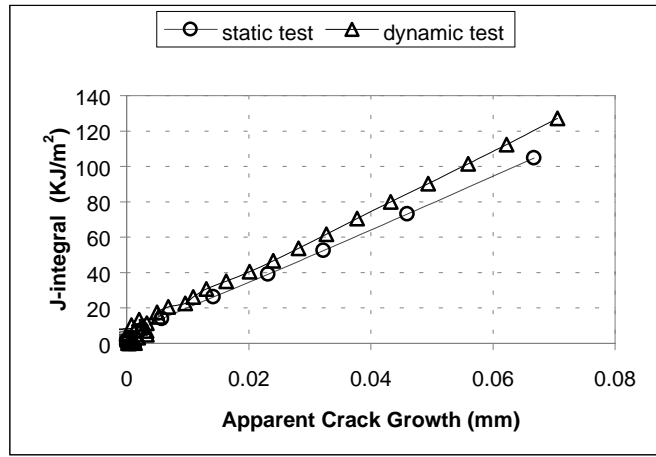


Figure 1: J-Damage curves



**Figure 2:** Numerical blunting lines

The SZW values corresponding to static and dynamic conditions are the same, and the fracture toughness parameters  $J_{SZW}$  and  $J^*_{SZW}$  are relatively close to one another in dynamic and static conditions. However the dynamic fracture parameters are higher than the static ones, which indicates the influence of strain rate. Comparing the values of  $J_{SZW}$  in static and dynamic conditions, which is a fracture parameter that takes the blunting effect into account experimentally, it can be concluded that the dynamic toughness for API X70 steel at the strain rates reached during the tests could be considered only slightly greater than that in the static conditions. To check the applicability of the damage model described to explain the difference between the static and dynamic fracture toughness, we made the following exercise: from the value of  $J_{szw}$ , obtained in the quasi-static test ( $76 \text{ kJ/m}^2$ ), a critical value of the damage variable, corresponding to the initiation of crack propagation, was calculated from Figure 1, which gave  $D_{crit} = 0.023$ . Since this material parameter is assumed as strain rate independent, and using Figure 1 again, values for the  $J_{szw}$ , but now in dynamic loading conditions, ranging from 80 to 90  $\text{kJ/m}^2$  were deduced, depending on the impact velocity of the test. These values are very close to that obtained experimentally for dynamic conditions ( $80 \text{ kJ/m}^2$ ), which illustrates the capacity of the micromechanical model to explain the fracture behaviour of the material involved as well as the apparent non-influence of strain rate on the parameter  $D_{crit}$ , at least at the intermediate values of strain rates reached in these tests.

## FRACTURE TEST AT HIGH STRAIN RATES

Although the Charpy impact test is the most widely used to evaluate the fracture initiation toughness,  $K_{Id}$ , the loading rates achieved in this test are limited to the order of  $\dot{K}_I = 10^5 \text{ MPa}\sqrt{\text{m}} / \text{s}$ . Some authors [10, 11] have suggested the use of special arrangements of the Split Hopkinson Bar to perform dynamic fracture tests at loading rates above  $\dot{K}_I = 10^6 \text{ MPa}\sqrt{\text{m}} / \text{s}$ . To measure the dynamic stress intensity factor, several optical [12-14] and photoelastic [15] techniques have been proposed. The following paragraphs describe a procedure to evaluate this parameter based on the direct measurement of the displacements of the specimen by means of a high speed photography technique. In this experimental method we modified the conventional Hopkinson bar device to carry out dynamic bending test at high strain rates.

### Experimental setup

The bending tests at high strain rate were performed using the experimental setup shown in Figure 3, with a striker bar, an input pressure bar, a supporting device and recording equipment. The specimen is placed between the input bar and the supporting device and is loaded to fracture by means of a concentrated transverse force applied at its midspan. The impact of the striker bar on the input bar at a velocity  $V_0$  generates a longitudinal compressive pulse that propagates along this bar. Part of this compressive pulse energy is transmitted to the specimen and the supporting device, while the rest of energy is reflected back to the input bar as a tensile pulse. From the one-dimensional elastic wave propagation theory, the input load and the displacement of the edge of

the bar initially in contact with the specimen may be calculated.

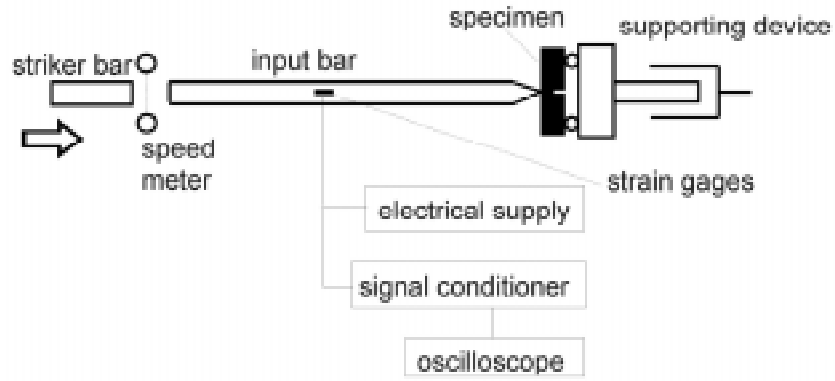


**Figure 3:** Experimental device for dynamic fracture test

Together with this device a system of high speed photography technique was used to measure the displacements of the specimen directly from the images. The system consists of four coupled CCD cameras, which can take images through the same objective with exposure times varying between 1  $\mu$ s and 1 ms. A more detailed description of the complete experimental arrangement can be found in reference [16].

#### **Material and experimental work**

The material used in our experiments was the aluminum alloy Al 7075-T651. Its chemical composition is shown in Table 3.

TABLE 3  
CHEMICAL COMPOSITION OF THE Al 7075-T651

Si	Fe	Cu	Mn	Mg	Cr	Zn	Ti
0.10	0.16	1.62	0.05	2.62	0.2	5.87	0.036

The Yield Stress and Ultimate Tensile Stress in static conditions of the material are, respectively,  $\sigma_y = 524$  MPa, and  $\sigma_u = 587$  MPa. Dynamic three-point bending tests were performed on specimens 20 mm height, 10 mm thick and 80 mm long according to ASTM E399 [17]. From the machined notch, an initial crack was generated by fatigue up to a total crack length,  $a_0$ , of 10 mm, approximately. Pre-cracking of the specimen was carried out according to ASTM E399 [17]. The crack length,  $a_0$ , is precisely measured on the fracture surface once the specimen is totally broken [17]. From the measures of the CMOD the dynamic stress intensity factor  $K_I^d$  can be evaluated using the same relation as that of the static case, i.e:

$$K_I = w_d \frac{E}{4(1-\nu^2)} \frac{\sqrt{W}}{a_0} \frac{\kappa(\beta, \alpha)}{h(\beta, \alpha)} \quad (8)$$

where  $w_d$  is the CMOD,  $E$  and  $\nu$  are, respectively, the Young modulus and Poisson coefficient. The functions  $\kappa(\beta, \alpha)$  and  $h(\beta, \alpha)$  depend on the ratios  $\beta = L/W$  ( $L$  is the span of the specimen) and  $\alpha = a_0/W$ . Their expressions for the case  $\beta = 4$  are [18]:

$$\kappa(\alpha) = \frac{\sqrt{\alpha}}{(1-\alpha)^{3/2}(1+3\alpha)} (1.9 + 0.41\alpha + 0.51\alpha^2 - 0.17\alpha^3) \quad (9)$$

$$h(\alpha) = 0.76 - 2.28\alpha + 3.78\alpha^2 - 2.04\alpha^3 + \frac{0.66}{(1-\alpha)^2} \quad (10)$$

The dynamic fracture initiation toughness,  $K_{I_d}$ , can be evaluated as the value of  $K_I^d$  at the instant of the beginning of crack propagation,  $t_f$ . This time, usually named time to fracture, was evaluated by a strain gage at the tip of the crack.

### Results and discussion

As an example of the results, Figure 4 shows the image of the crack mouth at different times during the test, taken by one of the four cameras. In this figure, the exposure time was 1  $\mu\text{s}$  and the time interval between two exposures was 10  $\mu\text{s}$

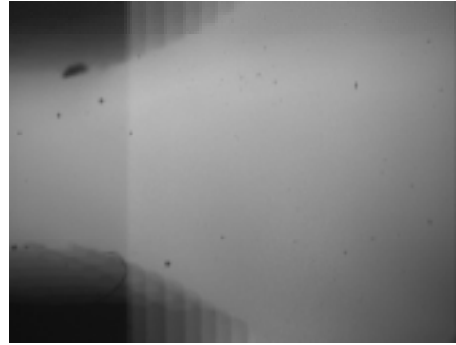


**Figure 4:** Evolution of CMOD during the test

From the CMOD values directly measured on the pictures and applying equations (8), (9) and (10) the variation of the dynamic stress intensity factor was evaluated. Figure 5 shows the variation of the dynamic stress intensity factor for a specimen tested, and Table 4 gives the results obtained for different specimens.

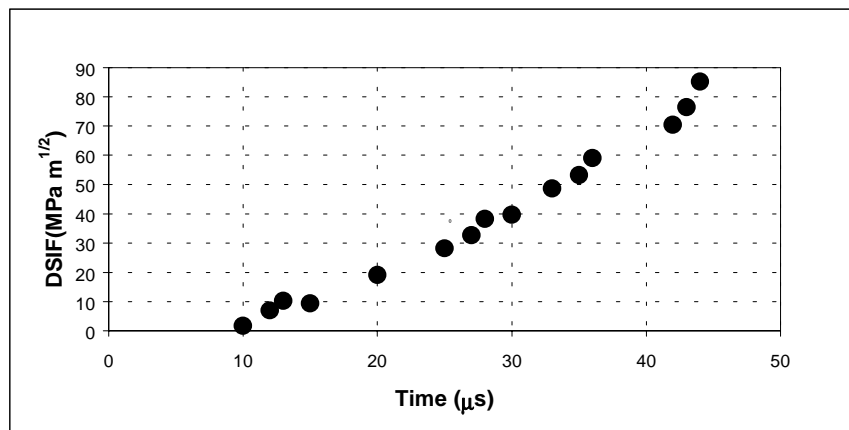


**Figure 5:** Evolution of the dynamic stress intensity factor (DSIF) during the test

TABLE 4  
EXPERIMENTAL RESULTS

Specimen	$a_0$ (mm)	$V_0$ (m/s)	$t_f$ ( $\mu\text{s}$ )	$K_{I_d}$
31	11.33	13.1	28	29
28	11.54	12.8	32	33
30	11.23	12.9	31	34
32	11.76	12.7	29	37
9	10.81	13.1	25	26
8	11.79	13.0	25	32
7	11.03	12.9	32	31
10	10.73	13.2	25	28
<b>Mean value</b>			28	31
<b>Standard deviation</b>			3.1	3.8

These results are similar to those obtained by others authors [11] for the same material and similar loading rate ( $\dot{K}_I = 10^6 \text{ MPa}\sqrt{\text{m}}/s$ ).

## SUMMARY

This work outlines recent developments at Carlos III University of Madrid in Dynamic Fracture Mechanics. Firstly we present some experimental and numerical studies of the fracture process for a ductile material. The influence of the strain rate on fracture initiation toughness of the material is explained using the micromechanical model of Rice and Tracey. Also the blunting process in dynamic conditions has been analysed. Secondly, some recent achievements in the field of the dynamic fracture test at high strain rates are shown. The experimental setup developed for this kind of test was based on a modified Split Hopkinson Pressure Bar and a system of high speed photography technique to measure the CMOD during the test directly from the images. From the CMOD measured just at the time to fracture, and assuming that the material presented elastic behaviour, the dynamic fracture initiation toughness can be obtained

## ACKNOWLEDGEMENTS

This work was partially supported by the Comisión Interministerial de Ciencia y Tecnología under Grant MAT96-0649. The authors wish to thank Dr. Amo and Dr. Durán of C.E.N.I.M for their good offices in procuring the API-X70 steel

## REFERENCES

1. Cornec, A., Heerens, J. and Schwalbe. (1986). GKSS Report 86/E/15
2. EGF P1-90,(1990). EGF Recommendations for determining the fracture resistance of ductile materials. European Group on Fracture.
3. MacGillivray and Lenkey, G.B. (1996). ECF11. :*Mechanisms and Mechanics of Damage and Failure*, pp. 2025-2030.
4. Joyce J.A. and Hacket, E.M. (1989). In : *ASTM STP 905*, American Society for Testing and Materials, pp. 741-774.
5. Yoon, J.H., Lee, B. S., Oh, Y. J. and Hong, J.H. (1999). *International Journal of Pressure Vessels and Piping*, **76**, 663
6. API Specification 5L. (1988). Specification for Line Pipe. American Petroleum Institute
7. de Luna, S. (1999). PhD. Thesis, . Universidad Carlos III de Madrid. Spain
8. Hibbit, Karlsson and Sorensen. (1998). Abaqus/Standard User's Manual, Version 5.8
9. Rice, J.R. and Tracey, D.M. (1969). *Journal of Applied Mechanics*, **17**;201.
10. Ruiz, C. And Mines, R.A.W. (1985). *International Journal of Fracture*, **29**, 101
11. Yokoyama, T. (1993). *Journal of Pressure Vessel Technology*, 115
12. Kalthoff, J.F. (1982). Proceedings of the International Conference on Experimental Stress Analysis, pp 1119-1126.
13. Ravi-Cahndar, K. and Knauss. (1984). W.G. *International Journal of Fracture*, **25**, 247.
14. Benítez, F.G. and Andrade, L. (1997). *Journal de Physique IV France*, **7**, C3-169
15. Dally, J.W. and Barker, D.B. (1988). *Experimental Mechanics*, **28**, 298.
16. Rubio, L. (1999). PhD. Thesis. Universidad Carlos III de Madrid. Spain
17. ASTM E 399 (1990). Standard Test Method for Plane-Strain Fracture Toughness of Metallic Materials. American Society for Testing and Materials
18. Guinea, G.V., Pastor, J.Y., Planas, J. And Elices, M. (1998). *International Journal of Fracture*, **89**, 103.